OPEN

NPG Asia Materials (2018) 10, e461; doi:10.1038/am.2017.212
www.nature.com/am

ORIGINAL ARTICLE

N-doped carbon nanotubes containing a high concentration of single iron atoms for efficient oxygen reduction

Jin-Cheng Li[1,5], Zhi-Qing Yang[1,5], Dai-Ming Tang[1,2], Lili Zhang[1], Peng-Xiang Hou[1], Shi-Yong Zhao[1], Chang Liu[1], Min Cheng[1], Guo-Xian Li[1], Feng Zhang[1] and Hui-Ming Cheng[1,3,4]

Fe-N-C has emerged as a promising noble-metal-free catalyst for the oxygen reduction reaction (ORR). However, achieving a catalytic activity comparable to that of Pt in acidic medium remains a great challenge. Here we report a N-doped carbon nanotube (CNT) catalyst in which a high concentration of single Fe atoms has been dispersed (CNT@Fe-N-PC). The catalyst was prepared by a simple and scalable atomic isolation method, in which a metal isolation agent was introduced to isolate Fe atoms and was then evaporated to produce abundant micropores that host single Fe atom active sites. The CNT@Fe-N-PC catalyst contained a high concentration of single Fe atom active sites and exhibited ultrahigh ORR activity with a half-wave potential of 0.82 V, comparable to that of Pt/C in an acidic medium. A high concentration of Fe-N_x active sites was created on a flexible single-wall CNT film and carbon cloth using this technique, and these materials showed even better ORR performance, that is, 40–60 mV more positive onset potentials than those of a commercial Pt/C catalyst. These catalysts exhibit excellent catalytic activity, good durability and low cost, and show great potential for commercial use as substitutes for current Pt-based catalysts.

NPG Asia Materials (2018) **10,** e461; doi:10.1038/am.2017.212; published online 12 January 2018

INTRODUCTION

Fuel cells, particularly proton exchange membrane fuel cells operated in an acidic medium, are considered one of the most promising electrochemical energy storage and conversion devices for transportation applications, due to their high theoretical specific energy, which is sufficient to power electric vehicles over a long driving range.[1–3] The sluggish oxygen reduction reaction (ORR) kinetics at the cathode in these devices compels us to use Pt-based catalysts to achieve desirable performance. However, the high cost, poor stability and low abundance of platinum limit the widespread use of Pt-based catalysts. Notable progress has been made in recent years in the development of low-cost noble-metal-free catalysts, including heteroatom-doped carbon materials,[4–6] Fe_3C-based materials[7–9] and transition-metal-coordinated nitrogen-doped carbon catalysts (Me-N-C, Me: Fe and/or Co).[10–12] Although these materials demonstrate desirable ORR catalytic activity comparable to that of Pt/C in an alkaline medium, only Me-N-C catalysts, particularly Fe-N-C, show relatively good catalytic activity and durability in acidic conditions,[13–15] which makes them attractive for use in proton exchange membrane fuel cells. Fe-N-C catalysts are generally synthesized by pyrolyzing precursors containing carbon, nitrogen, and iron at temperatures above 700 °C, to achieve high activity and a robust structure. Evidence shows that the ORR active sites of these catalysts are nitrogen-coordinated single iron atoms of the form Fe-N_x embedded in the basal planes of carbon or at the edges of two graphene planes and the average coordination number ranges from 2 to 4.[16–18] The catalyst activity is closely related to the concentration of active single Fe atom sites and previous work has aimed to increase the density of Fe-N_x sites by simply increasing the Fe concentration in the precursors during synthesis.[19] However, this approach is not effective because of the strong aggregation of Fe atoms that generates inactive Fe clusters and compounds. A high specific surface area is important for the ORR, because it is beneficial to both mass transport and the hosting of Fe-N_x sites. Thus, it has remained a great challenge to obtain Fe-N-C catalysts containing a high concentration of active Fe atoms that are uniformly dispersed in a carbon matrix with a high specific surface area.

To date, a three-step method of pyrolyzing precursors with electronegative N atoms anchoring electropositive Fe atoms (such as polyaniline-Fe, porphyrin-Fe and metal-organic framework) followed by long-term acidic leaching and further heat treatment has been developed and widely used to remove inactive Fe nanoparticles and increase the effective concentration of active single Fe atoms.[20–22] The

[1]Shenyang National Laboratory for Materials Science, Institute of Metal Research, Chinese Academy of Sciences, Shenyang, China; [2]World Premier International Center for Materials Nanoarchitectonics, National Institute for Materials Science, Ibaraki, Japan; [3]Tsinghua-Berkeley Shenzhen Institute (TBSI), Tsinghua University, Shenzhen, China and [4]Faculty of Science, Chemistry Department, King Abdulaziz University, Jeddah, Saudi Arabia
[5]These authors contributed equally to this work.
Correspondence: Professor P-X Hou or Professor C Liu, Institute of Metal Research, Chinese Academy of Sciences, 72 Wenhua Road, Shenyang 110016, China.
E-mail: pxhou@imr.ac.cn or cliu@imr.ac.cn
Received 3 April 2017; revised 31 August 2017; accepted 15 October 2017

above mentioned synthesis process is time-consuming and costly; therefore, it is not applicable for the large-scale fabrication of the catalyst.[23–25] Furthermore, it is inevitable that some active Fe-N_x sites are removed during the acid leaching process, thus compromising catalytic activity.[26] Most importantly, the performance of the catalyst obtained is still unsatisfactory, that is, the overpotential versus a commercial Pt/C catalyst is generally more than 60 mV.[20,27,28]

In this study, we developed a simple and scalable atomic isolation technique for synthesizing a porous Fe-N-C catalyst with a high concentration of N-coordinated single Fe atoms by pyrrole polymerization on carbon nanotubes (CNTs), followed by Fe^{3+} and Zn^{2+} (or Li^+, Na^+ and K^+) ion adsorption, and finally one-step pyrolysis. The resulting catalyst is denoted CNT@Fe-N-PC. Additional acid leaching and a second treatment are not required. During the pyrolysis, Fe atoms are uniformly dispersed with and spatially isolated by Zn atoms and directly converted to N-coordinated single Fe atoms, instead of large inactive Fe particles. Furthermore, pores are formed during the volatilization of the isolation Zn atoms; these pores are highly beneficial to ORR activity. As a result, the CNT@Fe-N-PC catalyst exhibits excellent ORR performance with a half-wave potential value of 0.82 V in an acidic medium, 20 mV more positive than that of Pt/C with a 'standard' loading of 0.1 mg cm^{-2} and only 20 mV more negative than that of Pt/C with the same loading of 0.3 mg cm^{-2}. The technique can be generalized to other carbon supports, including carbon black (CB), graphene oxide and flexible films of single-wall CNTs (SWCNTs, the resulting catalyst denoted SWCNT@Fe-N-PC film) or carbon cloth (CC, the resulting catalyst denoted CC@Fe-N-PC). Flexible SWCNT@Fe-N-PC and CC@Fe-N-PC films show even better ORR performance, with 40–60 mV more positive onset potentials than the onset potential of Pt/C loaded on CC. Considering the low cost and simplicity of this fabrication process, these high-efficiency, robust catalysts with a high concentration of single Fe atom sites are promising substitutes for noble Pt-based catalysts in proton exchange membrane fuel cells.

MATERIALS AND METHODS

Materials

CNTs were purchased from CNano Technology Ltd (Beijing, China). The chemicals used (potassium nitrate, potassium permanganate, concentrated sulfuric acid, 30% hydrogen peroxide solution, pyrrole, zinc nitrate hexahydrate, lithium chloride, sodium chloride, potassium chloride, anhydrous ferric chloride, hydrochloric acid and absolute ethyl alcohol) were of analytical grade and obtained from Sinopharm Chemical Reagent Co. Ltd (Shanghai, China). Potassium hydroxide (semiconductor grade, 99.99% trace metals basis) and perchloric acid (70%, 99.999% trace metal basis) were purchased from Sigma-Aldrich (St Louis, MO, USA). Platinum on CB (20 wt% of platinum) was purchased from Alfa Aesar (Haverhill, MA, USA). All chemicals were directly used without purification.

Synthesis of CNT@Fe-N-PC

In 18.75 ml of a 0.1 M hydrochloric acid solution, 37.5 mg of oxidized CNTs was dispersed and mixed with 0.75 ml pyrrole, followed by 10 min of sonication and 10 min of vigorous stirring. Subsequently, 18.75 ml of a solution containing 0.75 g ammonium peroxydisulfate (APS) was added dropwise to the abovementioned mixture under continuous stirring at room temperature. After stirring for 5 h to allow for polymerization, the product was separated by vacuum filtration and washed with ethanol and water. The wet hybrid was then dispersed in 100 ml of a mixture of zinc nitrate (0.4 M) and ferric chloride (10 mM), followed by 2 min of sonication and 10 h of vigorous stirring to allow it to adsorb Zn^{2+} and Fe^{3+} cations. Finally, this hybrid was collected by vacuum filtration, dried at 60 °C for 12 h and then pyrolyzed at 900 °C under a 200 standard cubic centimeter per minute Ar flow for 30 min and activated under 200 standard cubic centimeter per minute NH_3 flow for 30 min. The final CNT@Fe-N-PC catalyst was collected and cooled to room temperature under NH_3 flow.

Characterization of the CNT@Fe-N-PC catalyst

The catalysts were characterized using transmission electron microscopy (Titan G 60-300 S/TEM, 60 kV, FEI, Hillsboro, OR, USA; Tecnai F20, 200 kV, FEI, Hillsboro, OR, USA), X-ray photoelectron spectroscopy (Escalab 250, Al Kα) and X-ray diffraction (Rigaku diffractometer with CuKα radiation). The specific surface area and pore structure of the samples were investigated with an automatic volumetric sorption analyzer (ASAP 2020 M, Micromeritics Instrument Corporation, Norcross, GA, USA) using N_2 as the adsorbate at − 196 °C.

Electrochemical measurements

Electrochemical measurements were performed on an electrochemical analysis station (CHI 760 E, CH Instruments, Shanghai, China) using a standard three-electrode cell. A Pt wire and an Ag/AgCl electrode in a saturated KCl solution served as the counter electrode and reference electrode, respectively. All potential values refer to that of a reversible hydrogen electrode. A rotating disk electrode (RDE) with a glassy carbon disk (5.0 mm diameter) and a rotating RDE with a glass carbon disk (5.61 mm diameter) and a Pt ring (6.25 mm inner-diameter and 7.92 mm outer-diameter) were used as the substrate for the working electrode to evaluate the ORR performance. To prepare the working electrode, 4.0 mg of each catalyst was ultrasonically dispersed in ethanol containing 0.05 wt% Nafion (2.0 ml) to form a concentration of 2.0 mg ml^{-1} catalyst ink. The catalyst ink was then coated onto the surface of the glassy carbon disk for the RDE and rotating RDE tests. The non-noble-metal catalyst loading was 0.3 mg cm^{-2}. Pt/C (20 wt%, Alfa Aesar) with a 'standard' loading of 0.1 mg cm^{-2} and Pt/C with a 'high' loading of 0.3 mg cm^{-2} were used as reference samples. The materials' resistance to the methanol crossover effect and stability were evaluated using the same setup. The stability test was performed at 0.7 V in 0.1 M $HClO_4$ for chronoamperometry at room temperature at a working electrode rotation rate of 1600 r.p.m.

RESULTS

A schematic showing the fabrication process of the CNT@Fe-N-PC catalyst is shown in Figure 1a. In a typical procedure, functionalized CNTs (Supplementary Note 1) were dispersed in an aqueous HCl solution and pyrrole monomer was then added, followed by the dropwise addition of an APS solution to polymerize the pyrrole on the surface of the CNTs to form a CNT@polypyrrole (PPy) hybrid (step 1). After complete polymerization, the CNT@PPy hybrid was purified by vacuum filtration and washed with ethanol and water. The PPy/CNT hybrid was then dispersed in a 0.4 M $Zn(NO_3)_2$ solution containing a small amount of 10 mM $FeCl_3$ so that the hybrid material could adsorb Fe^{3+} and Zn^{2+}cations (step 2), which was confirmed by X-ray diffraction and X-ray photoelectron spectroscopy results (Supplementary Fig. 1a–c). The hybrid with adsorbed cations (CNT@PPy-Fe/Zn) was then pyrolyzed at 900 °C (step 3), an optimized calcination temperature in this study (Supplementary Fig. 2), during which the Zn evaporated and was deposited to form ZnO (Supplementary Fig. 1d). Meanwhile, abundant pores were generated, and a high concentration of active Fe-N_x sites was formed instead of the inactive Fe particles because of the spatial isolation effect of Zn.

Bright-field STEM characterization (Figure 1b) reveals that the CNT@Fe-N-PC catalyst has a 'core-shell' structure containing an outer shell of porous graphitized carbon with a thickness of <10 nm and an inner core of a multi-wall CNT with a diameter of ~ 15 nm. This structure does not only host abundant active Fe-N_x sites but also ensures excellent electrical conductivity, which is critical for high ORR catalytic activity. The X-ray diffraction pattern of the CNT@Fe-N-PC in Supplementary Fig. 3 shows peaks at 26° and 43° corresponding to the (002) and (101) planes of graphite, indicating that the CNT@Fe-N-PC catalyst has a high degree of graphitization and therefore high

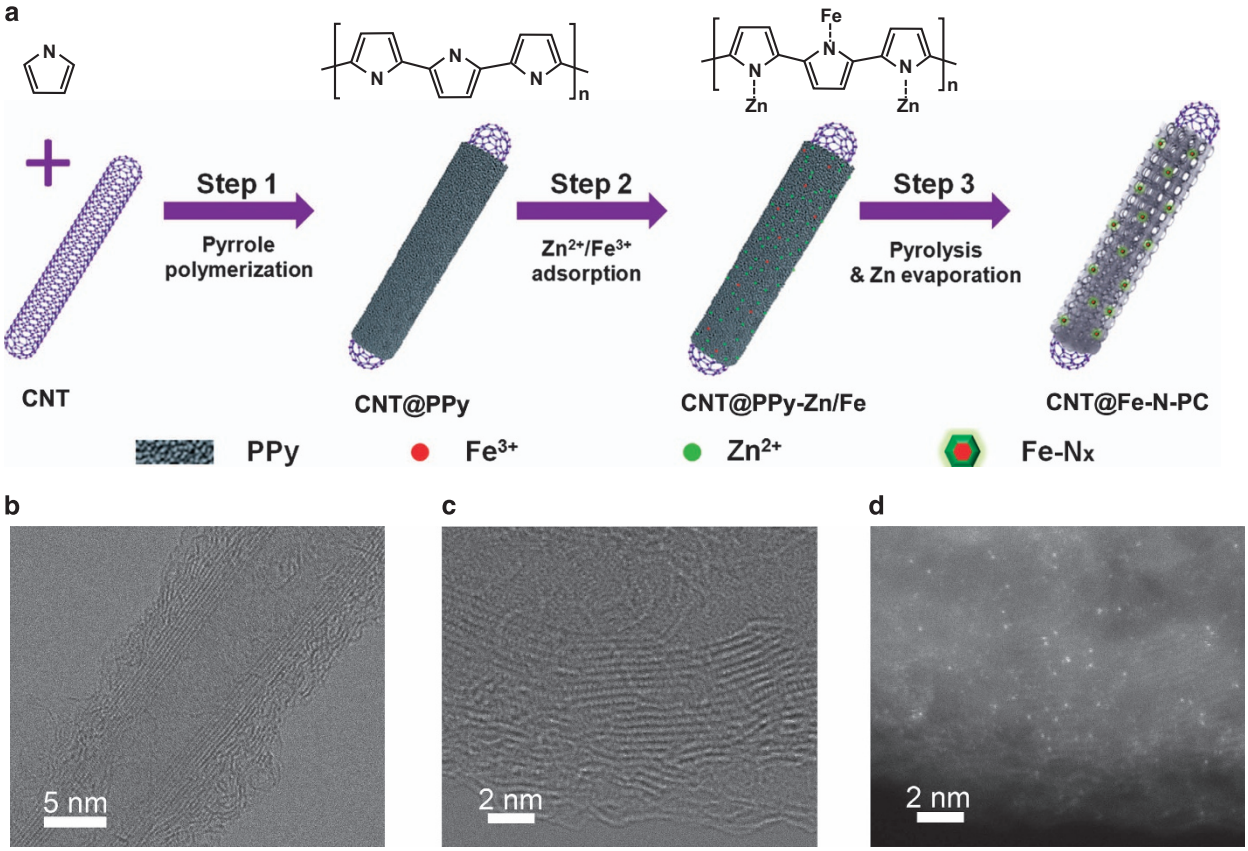

Figure 1 (**a**) Schematic showing the preparation of the CNT@Fe-N-PC catalyst. (**b**) Typical aberration-corrected low-magnification bright-field STEM (BF-STEM) image. (**c**) High-resolution BF-STEM image and (**d**) the corresponding Z-contrast image, demonstrating the presence of isolated heavy atoms in the CNT@Fe-N-PC catalyst.

electrical conductivity. Raman results show that the ratio of the intensity of the D-band to that of the G-band of CNT@Fe-N-PC is ~1.1 (Supplementary Fig. 4), further suggesting its high crystallinity and good electrical conductivity. To further verify the presence of a high concentration of single Fe atoms in the CNT@Fe-N-PC catalyst, we performed high-angle annular dark-field STEM (HAADF-STEM) imaging with simultaneous electron energy-loss spectroscopy analysis.[29,30] Isolated Fe atoms can be distinguished in the carbon support, as the atomic number, Z, of Fe is sufficiently higher than that of C. Figure 1c shows a high-resolution bright-field STEM image of the CNT@Fe-N-PC catalyst. Clearly, both the inner core of the CNT and the outer shell of the porous carbon are well crystallized. The HAADF-STEM image (Figure 1d) shows abundant and uniformly distributed isolated bright spots resulting from single heavy atoms. Core-loss electron energy-loss spectroscopy analysis shows a weak N signal (Supplementary Fig. 5), possibly because active Fe-N_x sites exist only on the surface of the catalyst. The bright spots are identified to be single Fe atoms based on the results of low-loss electron energy-loss spectroscopy performed in three regions with different numbers of bright atoms (Supplementary Fig. 6). Thus, we have directly confirmed that a large number of Fe atoms are uniformly dispersed in the nitrogen-doped carbon matrix, which is desirable for achieving a high-efficiency ORR.

Quantitative elemental analysis of the CNT@Fe-N-PC catalyst was performed by X-ray photoelectron spectroscopy. The C, O, N and Fe contents were determined to be 90.9 at.%, 3.3 at.%, 5.5 at.% and 0.3 at.%, respectively (Supplementary Table 1). Figure 2a shows the high-resolution N1s peaks of the CNT@Fe-N-PC and reference samples of iron phthalocyanine and PPy. Only one N 1*s* peak at ~398.7 eV can be observed for iron phthalocyanine, which originates from either Fe-N_x or pyridinic N because of the small difference in binding energy between Fe-N_x and pyridinic N.[31,32] Two separate N1*s* peaks were observed for PPy, which can be attributed to pyrrolic N (399.7 eV) and oxidized N (406.5 eV). The fitted peaks of the CNT@Fe-N-PC at 398.7 and 401.0 eV can be assigned to Fe-N_x (or pyridinic N, 23.7%) and graphitic N (76.3%), respectively.[33,34] This high Fe-N_x content confirms the existence of a high density of single Fe atom active sites, which is consistent with the HAADF-STEM results.

N_2 adsorption–desorption measurements were performed to reveal the pore structure of the CNT@Fe-N-PC catalyst. The type IV isotherm curve with hysteresis (Figure 2b) indicates the existence of mesopores. The rapid nitrogen uptake ($P/P_0 > 0.9$) can be ascribed to the presence of secondary large pores formed by the stacking of CNTs. Strong adsorption in the low-pressure ($P/P_0 = 0$–0.1) region and a small hysteresis loop in the medium-pressure ($P/P_0 = 0.45$–0.6) region are respectively attributed to abundant micropores and a small number of mesopores. Figure 2c shows the pore size distributions of the CNT@Fe-N-PC catalyst. Clearly, abundant micropores (pore size: <2 nm), very few mesopores (pore size: 5–50 nm) and macropores exist in the sample. The pore volume and Brunauer–Emmett–Teller (BET) surface area of the catalyst are 0.88 $cm^3\ g^{-1}$and 1180.2 $m^2\ g^{-1}$, respectively. It is believed that the high specific surface area and abundant porosity permit the accommodation of abundant active sites, and thus contribute to high ORR activity.[35] High porosity has

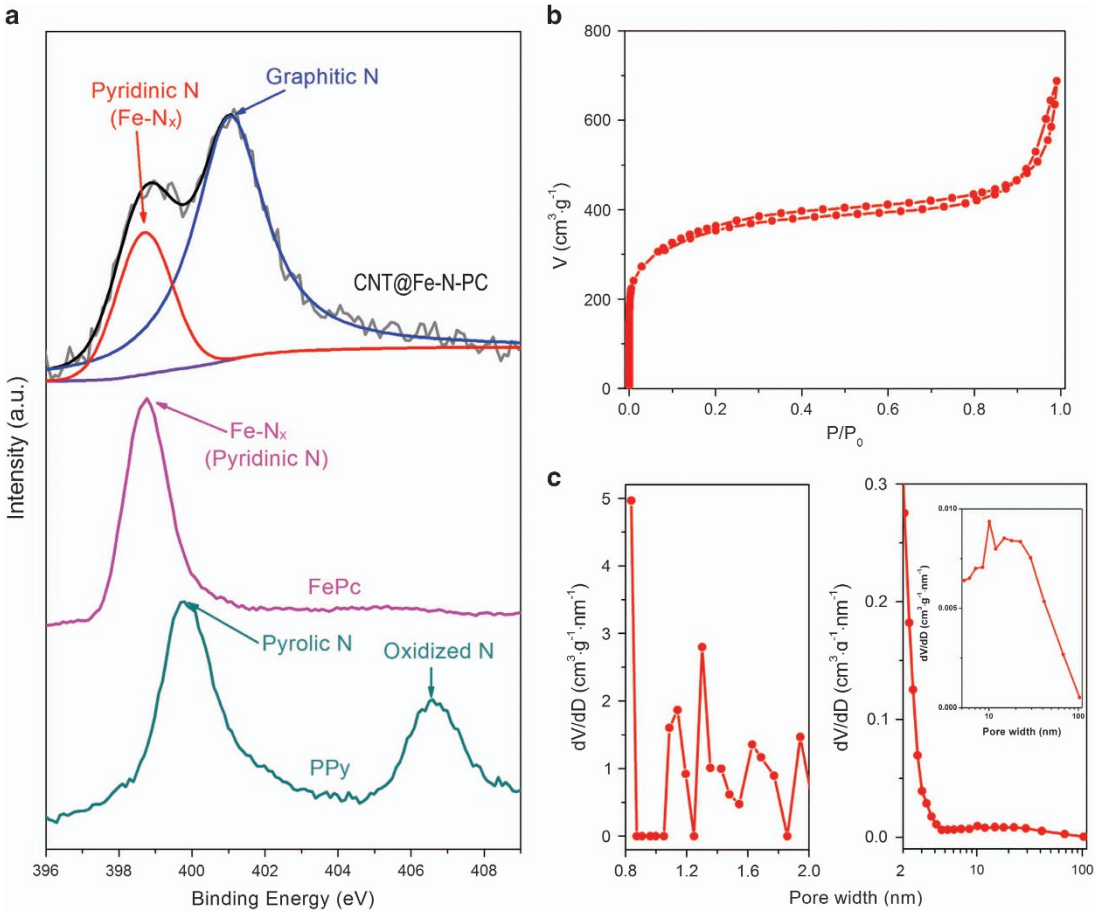

Figure 2 (**a**) High-resolution X-ray photoelectron spectroscopy (XPS) N 1*s* curves of the CNT@Fe-N-PC catalyst, iron phthalocyanine (FePc) and PPy. (**b**) N_2 adsorption–desorption isotherm and (**c**) the corresponding pore size distribution (the inset shows an enlarged view of the pore size distribution from 5 to 100 nm) of the CNT@Fe-N-PC catalyst.

been identified as being favorable for efficient mass transfer and minimizing the ion diffusion distance.[25] The CNT@Fe-N-PC catalyst prepared has a high BET surface area, high pore volume and high content of Fe-N_x sites, and can therefore be reasonably expected to display excellent ORR performance.

The electrocatalytic activity of the CNT@Fe-N-PC catalyst for the ORR was evaluated by rotating ring-disk electrode (RRDE) measurements in an O_2-saturated 0.1 M $HClO_4$ solution. As shown in Figure 3a, the CNT@Fe-N-PC catalyst shows a positive half-wave potential ($E_{1/2}$) of ~0.82 V and a large limiting current density (j_L) of ~6.3 mA cm^{-2}. The HO_2^- yield at all potentials is <3% and decreases to below 1% at 0.2 V. The low HO_2^- yield shows that the catalyst has high catalytic efficiency for the ORR under acidic conditions and follows a complete four-electron-transfer pathway (Supplementary Fig. 7). A commercial Pt/C catalyst (20 wt% Pt, Alfa Aesar) with a 'standard' loading[20] of 0.1 mg cm^{-2} was used as a reference material and its catalytic activity is clearly poorer than that of the CNT@Fe-N-PC catalyst (Figure 3a), showing a more negative $E_{1/2}$ of 0.80 V and a smaller j_L of 5.2 mA cm^{-2}. Even when compared with Pt/C with the same loading of 0.3 mg cm^{-2}, the CNT@Fe-N-PC catalyst has only a slightly smaller $E_{1/2}$ value of 0.02 V. Kinetic currents derived from the mass transport correction of the disk current (Figure 3b) show that the CNT@Fe-N-PC catalyst has a Tafel slope of 67 mV/decade, smaller than that of Pt/C (80 mV/decade), indicating that the catalyst has even better ORR kinetics, and that the transfer of the first electron is likely the rate-determining step.[36] Subsequently, rotating disk electrode (RDE) measurements of the CNT@Fe-N-PC catalyst at different rotation rates (ranging from 400 to 2000 r.p.m.) were performed (Supplementary Fig. 8a). Supplementary Fig. 8b shows that the average value of the electron-transfer number for the CNT@Fe-N-PC catalyst is ~4.0 based on the Koutecky–Levich equation, further revealing that its ORR follows a complete four-electron-transfer pathway. To the best of our knowledge, our CNT@Fe-N-PC catalyst showed the best ORR performance in an acidic medium compared with all previously reported Fe-N-C and other non-noble-metal catalysts (Supplementary Table 2).[11,12,13,20,22,27,28,31,37–40]

In addition to the high activity, we further studied the durability of the CNT@Fe-N-PC catalyst. Figure 3c shows that the current density decay is 12% after 40 000 s of testing, much smaller than that (57%) of commercial Pt/C. In addition, the linear sweep voltammetry polarization curves (Figure 3d) before and after 40 000 s of testing show that $E_{1/2}$ has a small negative shift of ~20 mV, which outperforms that of Pt/C (negative shift: ~130 mV). Furthermore, we characterized the CNT@Fe-N-PC catalyst by HAADF-STEM imaging after ORR tests and it was found that the density of single Fe atoms remained nearly unchanged compared with that observed before ORR tests (Supplementary Fig. 9), which indicates a high stability of the Fe-N_x active sites under acidic conditions. These results indicate that the CNT@Fe-N-PC catalyst possesses excellent durability in an acidic

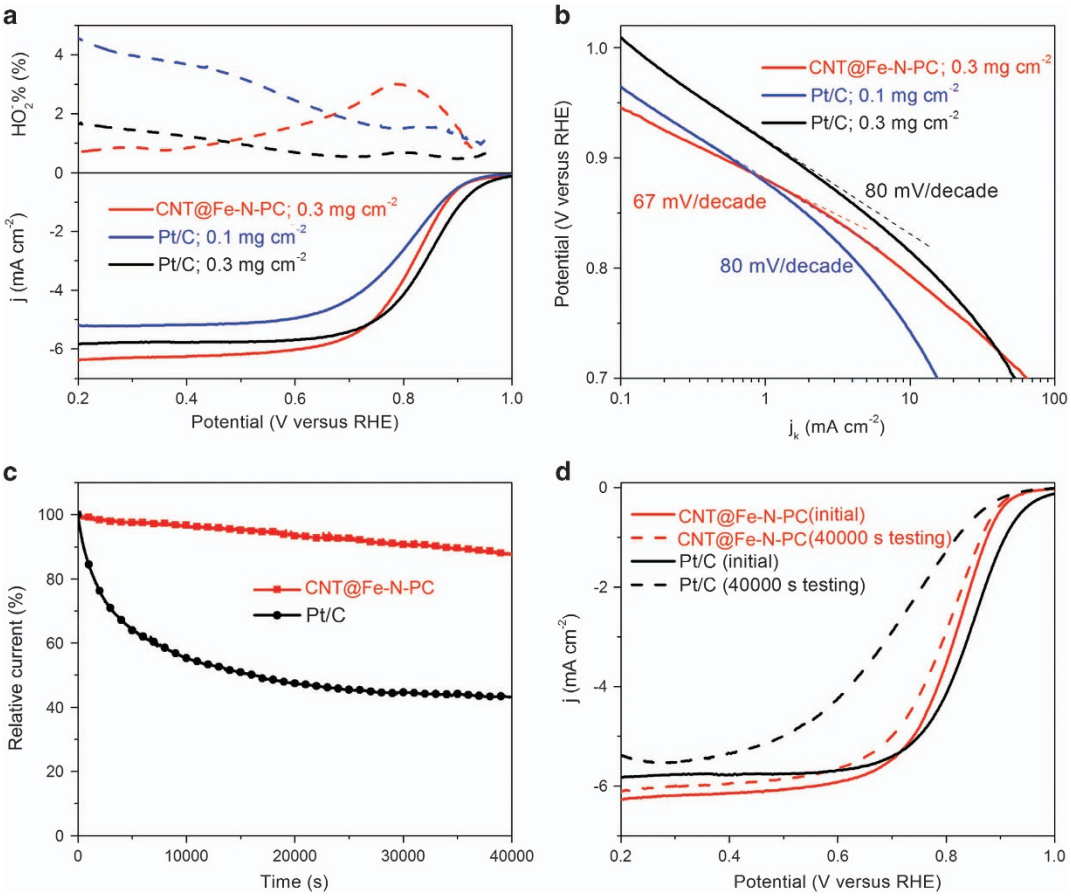

Figure 3 (**a**) RRDE polarization curves and peroxide yield of the CNT@Fe-N-PC catalyst with a loading of 0.3 mg cm^{-2} and those of Pt/C with loadings of 0.1 and 0.3 mg cm^{-2} in an O_2-saturated 0.1 M $HClO_4$. (**b**) Tafel plots of the CNT@Fe-N-PC and Pt/C catalysts. (**c**) Stability evaluation tested by chronoamperometric responses. (**d**) Linear sweep voltammetry curves of the CNT@Fe-N-PC and Pt/C catalysts before and after the chronoamperometric responses. Electrode rotation speed: 1600 r.p.m.; scan rate: 5 mV s^{-1}.

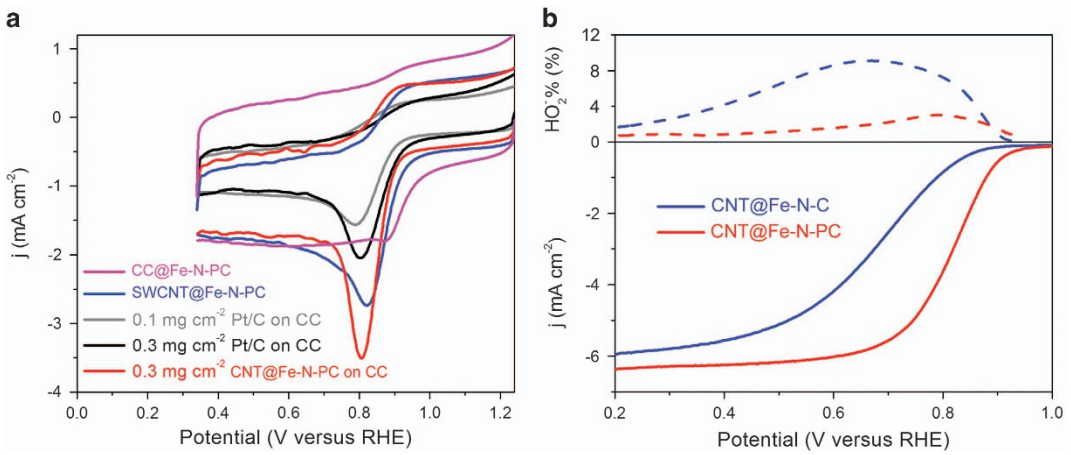

Figure 4 (**a**) Cyclic voltammetric curves of the CC@Fe-N-PC catalyst, a SWCNT@Fe-N-PC film, CNT@Fe-N-PC on CC and Pt/C with different loadings on CC. Scan rate: 5 mV s^{-1}. (**b**) RRDE polarization curves and peroxide yield of the CNT@Fe-N-C and CNT@Fe-N-PC catalysts with a loading of 0.3 mg cm^{-2}.

medium. Subsequently, the tolerance of the CNT@Fe-N-PC and Pt/C catalysts towards methanol was determined by adding 0.1 M methanol during chronoamperometric measurements. As shown in Supplementary Fig. 10, the current density of the CNT@Fe-N-PC catalyst remained nearly unchanged, whereas that of the Pt/C catalyst sharply decreased upon the addition of methanol, suggesting that the CNT@Fe-N-PC catalyst is free of methanol crossover.

An optimal Fe content is the key to obtaining a high-activity CNT@Fe-N-PC catalyst. We therefore investigated the effect of the ratio of Fe^{3+} to Zn^{2+} on the ORR activity of the obtained CNT@Fe-N-

PC catalysts (denoted 1, 0:400; 2, 5:400; 3, 10:400; 4, 15:400). It was observed that the catalyst without Fe (1) showed poor ORR activity (Supplementary Fig. 11). With the increase in the Fe/Zn ratio (2 and 3), the ORR activity improved appreciably, which suggests that the primary active sites are Fe-N_x instead of N-doped carbon, because these catalysts have a similar morphology and pore structure (Supplementary Table 1). However, the ORR activity of sample 4 was worse, possibly because a further increase in Fe content results in the formation of inactive Fe clusters (Supplementary Fig. 11).

Furthermore, our method can be generalized to other carbon supports. Supplementary Fig. 12 shows that iron atoms dispersed in CB (CB@Fe-N-PC) and graphene oxide (GO@Fe-N-PC) also show a high ORR catalytic activity. In addition, it was previously reported that flexible CC and SWCNT films can be used as a gas diffusion layer, where powder catalysts were loaded onto them using Nafion glue.[17,41,42] However, the use of glue leads to additional resistance and the loss of some active sites because they are submerged in the glue.[43] These findings motivated us to prepare flexible CC@Fe-N-PC and SWCNT@Fe-N-PC films (Supplementary Fig. 13) with a high concentration of active sites that can be directly used as electrodes. The ORR activity of the materials obtained was evaluated through cyclic voltammetric tests (Figure 4a). Remarkably, the CC@Fe-N-PC and SWCNT@Fe-N-PC film electrodes showed outstanding ORR activities with onset potentials of 1.07 and 1.05 V (Supplementary Fig. 14), respectively, even more positive than those of the CNT@Fe-N-PC (1.01 V) and Pt/C catalyst with loadings of 0.1 mg cm^{-2} (1.00 V) and 0.3 mg cm^{-2} (1.01 V) on a CC support. In addition, the ORR peak potential for the CC@Fe-N-PC (0.870 V) and SWCNT@Fe-N-PC (0.822 V) films was higher than those of the CNT@Fe-N-PC (0.807 V) and Pt/C catalyst (0.1 mg cm^{-2} loading: 0.790 V; 0.3 mg cm^{-2} loading: 0.804 V) on CC. The CC@Fe-N-PC and SWCNT@Fe-N-PC films showed even better ORR performance than the CC with Pt/C powder or CNT@Fe-N-PC glued. This discrepancy was observed mainly because additional resistance originating from the poor electrical conductivity of binders and the large interface resistance for the latter are avoided. In addition, the active sites can be more efficiently used when they and the conductive support are combined without using any glue. Considering that our method is very simple and scalable, the raw materials used are inexpensive and the achieved ORR performance is much better than that of Pt/C, we believe that this is one of the most efficient methods for synthesizing noble-metal-free catalysts with outstanding ORR activity beyond that of a Pt-based catalyst.

The introduction of Zn into the precursor is a key step to obtaining a high-efficiency CNT@Fe-N-PC catalyst for the ORR. To investigate the effect of Zn on the activity of the catalyst obtained, we used a CNT@PPy hybrid to adsorb Fe^{3+} rather than Fe^{3+}/Zn^{2+}, whereas the

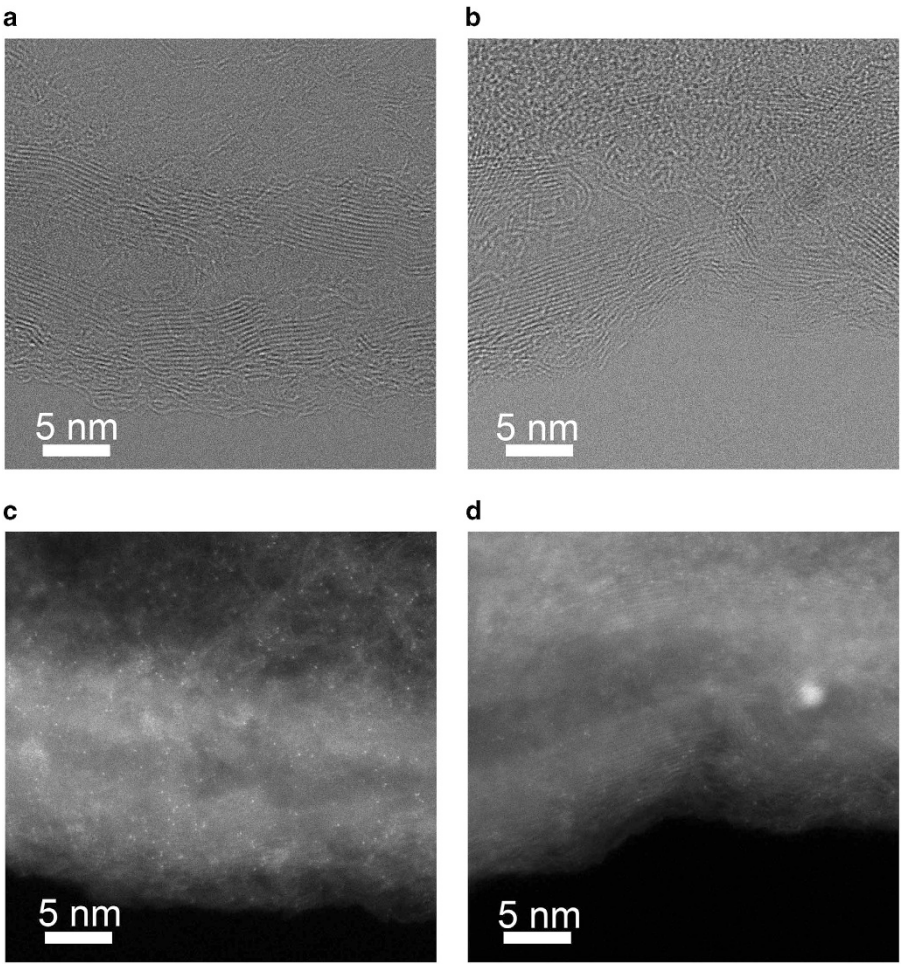

Figure 5 BF-STEM images of the (**a**) CNT@Fe-N-PC and (**b**) CNT@Fe-N-C catalysts. The corresponding Z-contrast images of the (**c**) CNT@Fe-N-PC and (**d**) CNT@Fe-N-C catalysts show different concentrations of single Fe atoms.

other conditions were kept unchanged; this catalyst is denoted CNT@Fe-N-C. Substantial decreases in BET surface area and pore volume from 1180.2 to 408.2 $m^2 g^{-1}$ and 0.88 to 0.28 $cm^3 g^{-1}$, respectively, were identified by N_2 adsorption–desorption characterization (Supplementary Fig. 15). These results well verify that the introduction of Zn is critical for the creation of abundant pores by evaporation. X-ray photoelectron spectroscopy analysis of the CNT@Fe-N-C catalyst reveals that the N content decreased slightly compared with that of the CNT@Fe-N-PC catalyst (Supplementary Table 1), whereas the concentration of active Fe-N_x (or pyridinic N) sites decreased from 23.7% to 18.3% (Supplementary Fig. 16). This result further suggests that Fe atoms are spatially isolated by the surrounding Zn atoms and consequently inhibit the agglomeration of Fe atoms. Figure 4b shows the rotating RDE curve of a CNT@Fe-N-C electrode for the ORR recorded at 1600 r.p.m. in 0.1 M $HClO_4$. Clearly, the CNT@Fe-N-C shows ordinary ORR catalytic activity with a HO_2^- yield below 10% and an $E_{1/2}$ of ~0.68 V, 140 mV more negative than that of CNT@Fe-N-PC. The poor ORR catalytic activity of CNT@Fe-N-C is primarily attributed to its low BET surface area, which supports only a low concentration of active Fe-N_x sites.

To further verify the isolation effect of Zn on Fe atom distribution, we performed bright-field STEM and HAADF-STEM imaging to show the microstructure of the carbon matrix and the single Fe atoms incorporated into each sample. The bright-field STEM images of both CNT@Fe-N-PC (Figure 5a) and CNT@Fe-N-C (Figure 5b) show a similar microstructure of highly crystallized CNTs intimately linked with porous carbon. However, the corresponding HAADF-STEM images of the CNT@Fe-N-PC (Figure 5c) and CNT@Fe-N-C catalysts (Figure 5d) are quite different. The CNT@Fe-N-PC catalyst shows a uniform distribution of isolated Fe atoms with a density of ~30 ± 3 atoms per 100 square nanometer, which is more than six times higher than that of CNT@Fe-N-C. This result indicates that Zn has an important role in promoting the formation of a high concentration of single Fe atom sites, which significantly improves the ORR catalytic activity.

In addition to $Zn(NO_3)_2$, we also tried using MCl (M = Li, Na and K) as isolating agents to prepare a CNT@Fe-N-PC catalyst with a high density of active Fe sites because of their chemical inertness to Fe and water solubility. The catalysts derived from MCl also showed high BET surface areas (Supplementary Fig. 17a) and active Fe-N_x sites (Supplementary Fig. 17b), and demonstrated excellent ORR catalytic activity (Supplementary Fig. 18), particularly the catalyst derived from LiCl, which showed an $E_{1/2}$ of ~0.815 V, slightly more negative than that of the CNT@Fe-N-PC catalyst (0.820 V). This finding reveals that alkali salts are also promising isolating agents for preparing Fe-N-C catalysts with a high density of active Fe sites. Furthermore, with an increase in the atomic number of alkali metal in MCl isolating agents, the BET surface areas (Supplementary Fig. 17a) and ORR performance (Supplementary Fig. 18) of the obtained materials decrease. An increase in the atomic radius of the alkali metal in isolating agents may result in weaker interactions with carbon materials, lower BET surface areas of the final products and, therefore, degraded ORR performance.

DISCUSSION

The superior ORR performance of CNT@Fe-N-PC catalysts unambiguously demonstrates the importance of a high density of active sites, high BET surface area and high electrical conductivity. With the introduction of atom-isolating agents, Fe atoms adsorbed by electronegative N atoms can be directly converted to active Fe-N_x sites rather than inactive Fe clusters. Furthermore, abundant pores form upon the removal of the atom-isolating agents. Interestingly, CNT@Fe-N-PC catalysts with a tunable BET surface area and pore structures can be obtained (Figure 2b and Supplementary Fig. 17a) by introducing different atom-isolating agents and these catalysts therefore show different ORR catalytic activities (Figure 3a and Supplementary Fig. 18). In addition, conductive supports are important for achieving good ORR activity. When CNTs were used as the support, the catalyst showed better ORR performance than that of CB and graphene oxide (Supplementary Fig. 12).

In summary, we developed a simple and cost-effective atom isolation technique for fabricating CNT@Fe-N-PC catalysts with a high BET surface area and uniformly distributed micropores that can host a high concentration of single Fe atom active sites. An atom-isolating agent (such as $Zn(NO_3)_2$, LiCl, NaCl and KCl) was used to effectively produce a high density of single Fe atom active sites and to increase the exposed surface area of the catalysts by evaporation during pyrolysis or water washing. As a result, the CNT@Fe-N-PC exhibits outstanding ORR catalytic activity with an $E_{1/2}$ of 0.82 V, which is comparable to that of Pt/C in an acidic medium. A flexible SWCNT@Fe-N-PC film and CC@Fe-N-PC fabricated following this strategy show much better ORR performance than that of commercial Pt/C catalysts. Considering their low cost, excellent catalytic activity and good durability, these catalysts have great potential for use in the ORR, serving as substitutes for Pt-based catalysts.

CONFLICT OF INTEREST

The authors declare no conflict of interest.

ACKNOWLEDGEMENTS

This work was supported by the Ministry of Science and Technology of China (Grant 2016YFA0200102), the National Natural Science Foundation of China (Grants 51625203, 51532008, 51521091 and 51572264), the Chinese Academy of Sciences (Grant KGZD-EW-T06), the CAS/SAFEA International Partnership Program for Creative Research Teams and the Liaoning BaiQianWan Talents Program. DMT acknowledges Dr Ovidiu Cretu and the TEM Station of NIMS, Japan, for their help in the characterization of single iron atoms.

1 Debe, M. K. Electrocatalyst approaches and challenges for automotive fuel cells. *Nature* **486**, 43–51 (2012).
2 Xia, W., Mahmood, A., Liang, Z., Zou, R. & Guo, S. Earth-abundant nanomaterials for oxygen reduction. *Angew. Chem. Int. Ed.* **55**, 2650–2676 (2016).
3 He, W., Wang, Y., Jiang, C. & Lu, L. Structural effects of a carbon matrix in non-precious metal O_2-reduction electrocatalysts. *Chem. Soc. Rev.* **45**, 2396–2409 (2016).
4 Gong, K., Du, F., Xia, Z., Durstock, M. & Dai, L. Nitrogen-doped carbon nanotube arrays with high electrocatalytic activity for oxygen reduction. *Science* **323**, 760–764 (2009).
5 Chen, S., Bi, J., Zhao, Y., Yang, L., Zhang, C., Ma, Y., Wu, Q., Wang, X. & Hu, Z. Nitrogen-doped carbon nanocages as efficient metal-free electrocatalysts for oxygen reduction reaction. *Adv. Mater.* **24**, 5593–5597 (2012).
6 Liang, J., Du, X., Gibson, C., Du, X. W. & Qiao, S. Z. N-doped graphene natively grown on hierarchical ordered porous carbon for enhanced oxygen reduction. *Adv. Mater.* **25**, 6226–6231 (2013).
7 Yang, W., Liu, X., Yue, X., Jia, J. & Guo, S. Bamboo-like carbon nanotube/Fe_3C nanoparticle hybrids and their highly efficient catalysis for oxygen reduction. *J. Am. Chem. Soc.* **137**, 1436–1439 (2015).
8 Hu, Y., Jensen, J. O., Zhang, W., Cleemann, L. N., Xing, W., Bjerrum, N. J. & Li Qingfeng. Hollow spheres of iron carbide nanoparticles encased in graphitic layers as oxygen reduction catalysts. *Angew. Chem. Int. Ed.* **53**, 3675–3679 (2014).
9 Wu, Z. Y., Xu, X. X., Hu, B. C., Liang, H. W., Lin, Y., Chen, L. F. & Yu, S. H. Iron carbide nanoparticles encapsulated in mesoporous Fe-N-doped carbon nanofibers for efficient electrocatalysis. *Angew. Chem. Int. Ed.* **54**, 8179–8183 (2015).
10 Liang, J., Zhou, R. F., Chen, X. M., Tang, Y. H. & Qiao, S. Z. Fe–N decorated hybrids of CNTs grown on hierarchically porous carbon for high-performance oxygen reduction. *Adv. Mater.* **26**, 6074–6079 (2014).
11 Li, J. C., Hou, P. X., Shi, C., Zhao, S. Y., Tang, D. M., Cheng, M., Liu, C. & Cheng, H. M. Hierarchically porous Fe-N-doped carbon nanotubes as efficient electrocatalyst for oxygen reduction. *Carbon* **109**, 632–639 (2016).

12 Yasuda, S., Furuya, A., Uchibori, Y., Kim, J. & Murakoshi, K. Iron–nitrogen-doped vertically aligned carbon nanotube electrocatalyst for the oxygen reduction reaction. *Adv. Funct. Mater.* **26**, 738–744 (2016).
13 Yang, G., Choi, W., Xiong, P. & Yu, C. Scalable synthesis of bi-functional high-performance carbon nanotube sponge catalysts and electrodes with optimum C-N-Fe coordination for oxygen reduction reaction. *Energy Environ. Sci.* **8**, 1799–1807 (2015).
14 Lin, Q., Bu, X., Kong, A., Mao, C., Zhao, X., Bu, F. & Feng, P. New heterometallic zirconium metalloporphyrin frameworks and their heteroatom-activated high-surface-area carbon derivatives. *J. Am. Chem. Soc.* **137**, 2235–2238 (2015).
15 Gasteiger, H. A. & Marković, N. M. Just a dream—or future reality? *Science* **324**, 48–49 (2009).
16 Zitolo, A., Goellner, V., Armel, V., Sougrati, M. T., Mineva, T., Stievano, L., Fonda, E. & Jaouen, F. Identification of catalytic sites for oxygen reduction in iron- and nitrogen-doped graphene materials. *Nat. Mater.* **14**, 937–942 (2015).
17 Lefèvre, M., Proietti, E., Jaouen, F. & Dodelet, J. P. Iron-based catalysts with improved oxygen reduction activity in polymer electrolyte fuel cells. *Science* **324**, 71–74 (2009).
18 Palaniselvam, T., Kashyap, V., Bhange, S. N., Baek, J. B. & Kurungot, S. Nanoporous graphene enriched with Fe/Co-N active sites as a promising oxygen reduction electrocatalyst for anion exchange membrane fuel cells. *Adv. Funct. Mater.* **26**, 2150–2162 (2016).
19 Jaouen, F. & Dodelet, J. P. Average turn-over frequency of O_2 electro-reduction for Fe/N/C and Co/N/C catalysts in PEFCs. *Electrochim. Acta* **52**, 5975–5984 (2007).
20 Wu, G., More, K. L., Johnston, C. M. & Zelenay, P. High-performance electrocatalysts for oxygen reduction derived from polyaniline, iron, and cobalt. *Science* **332**, 443–447 (2011).
21 Sahraie, N. R., Kramm, U. I., Steinberg, J., Zhang, Y., Thomas, A., Reier, T., Paraknowitsch, J. P. & Strasser, P. Quantifying the density and utilization of active sites in non-precious metal oxygen electroreduction catalysts. *Nat. Commun.* **6**, 8618 (2015).
22 Yuan, S., Shui, J. L., Grabstanowicz, L., Chen, C., Commet, S., Reprogle, B., Xu, T., Yu, L. & Liu, D. J. A highly active and support-free oxygen reduction catalyst prepared from ultrahigh-surface-area porous polyporphyrin. *Angew. Chem. Int. Ed.* **52**, 8349–8353 (2013).
23 Wang, Q., Zhou, Z. Y., Lai, Y. J., You, Y., Liu, J. G., Wu, X. L., Terefe, E., Chen, C., Song, L., Rauf, M., Tian, N. & Sun, S. G. Phenylenediamine-based FeNx/C catalyst with high activity for oxygen reduction in acid medium and its active-site probing. *J. Am. Chem. Soc.* **136**, 10882–10885 (2014).
24 Peng, H., Mo, Z., Liao, S., Liang, H., Yang, L., Luo, F., Song, H., Zhong, Y. & Zhang, B. High performance Fe- and N- doped carbon catalyst with graphene structure for oxygen reduction. *Sci. Rep.* **3**, 1765 (2013).
25 Li, J. C., Zhao, S. Y., Hou, P. X., Fang, R. P., Liu, C., Liang, J., Luan, J., Shan, X. Y. & Cheng, H. M. A nitrogen-doped mesoporous carbon containing an embedded network of carbon nanotubes as a highly efficient catalyst for the oxygen reduction reaction. *Nanoscale* **7**, 19201–19206 (2015).
26 Jiang, W. J., Gu, L., Li, L., Zhang, Y., Zhang, X., Zhang, L. J., Wang, J. Q., Hu, J. S., Wei, Z. & Wan, L. J. Understanding the high activity of Fe–N–C electrocatalysts in oxygen reduction: Fe/Fe_3C nanoparticles boost the activity of $Fe–N_x$. *J. Am. Chem. Soc.* **138**, 3570–3578 (2016).
27 Ding, W., Li, L., Xiong, K., Wang, Y., Li, W., Nie, Y., Chen, S., Qi, X. & Wei, Z . Shape fixing via salt recrystallization: a morphology-controlled approach to convert nanostructured polymer to carbon nanomaterial as a highly active catalyst for oxygen reduction reaction. *J. Am. Chem. Soc.* **137**, 5414–5420 (2015).
28 Strickland, K., Miner, E., Jia, Q., Tylus, U., Ramaswamy, N., Liang, W., Sougrati, M. T., Jaouen, F. & Mukerjee, S. Highly active oxygen reduction non-platinum group metal electrocatalyst without direct metal-nitrogen coordination. *Nat. Commun.* **6** (2015).
29 Pennycook, S. J. Z-contrast stem for materials science. *Ultramicroscopy* **30**, 58–69 (1989).
30 Yin, P., Yao, T., Wu, Y., Zheng, L., Lin, Y., Liu, W., Ju, H., Zhu, J., Hong, X., Deng, Z., Zhou, G., Wei, S. & Li, Y. Single cobalt atoms with precise N-coordination as superior oxygen reduction reaction catalysts. *Angew. Chem. Int. Ed.* **55**, 10800–10805 (2016).
31 Liang, H. W., Wei, W., Wu, Z. S., Feng, X. & Müllen, K. Mesoporous metal–nitrogen-doped carbon electrocatalysts for highly efficient oxygen reduction reaction. *J. Am. Chem. Soc.* **135**, 16002–16005 (2013).
32 Hijazi, I., Bourgeteau, T., Cornut, R., Morozan, A., Filoramo, A., Leroy, J., Derycke, V., Jousselme, B. & Campidelli, S. Carbon nanotube-templated synthesis of covalent porphyrin network for oxygen reduction reaction. *J. Am. Chem. Soc.* **136**, 6348–6354 (2014).
33 Li, J. C., Hou, P. X., Zhang, L., Liu, C. & Cheng, H. M. Growth of metal-catalyst-free nitrogen-doped metallic single-wall carbon nanotubes. *Nanoscale* **6**, 12065–12070 (2014).
34 Zhu, Y., Zhang, B., Liu, X., Wang, D. W. & Su, D. S. Unravelling the structure of electrocatalytically active Fe–N complexes in carbon for the oxygen reduction reaction. *Angew. Chem. Int. Ed.* **53**, 10673–10677 (2014).
35 Liang, H. W., Zhuang, X., Brüller, S., Feng, X. & Müllen, K. Hierarchically porous carbons with optimized nitrogen doping as highly active electrocatalysts for oxygen reduction. *Nat. Commun.* **5**, 4973 (2014).
36 Li, Y., Zhou, W., Wang, H., Xie, L., Liang, Y., Wei, F., Idrobo, J. C., Pennycook, S. J. & Dai, H. An oxygen reduction electrocatalyst based on carbon nanotube-graphene complexes. *Nat. Nanotechnol.* **7**, 394–400 (2012).
37 Zhou, M., Yang, C. & Chan, K. Y. Structuring porous iron-nitrogen-doped carbon in a core/shell geometry for the oxygen reduction reaction. *Adv. Energy Mater.* **4**, 1400840 (2014).
38 Muthukrishnan, A., Nabae, Y., Okajima, T. & Ohsaka, T. Kinetic approach to investigate the mechanistic pathways of oxygen reduction reaction on Fe-containing N-doped carbon catalysts. *ACS Catal.* **5**, 5194–5202 (2015).
39 Wang, X., Zhang, H., Lin, H., Gupta, S., Wang, C., Tao, Z., Fu, H., Wang, T., Zheng, J., Wu, G. & Li, X. Directly converting Fe-doped metal–organic frameworks into highly active and stable Fe-N-C catalysts for oxygen reduction in acid. *Nano Energy* **25**, 110–119 (2016).
40 Zhao, D., Zhao, D., Shui, J. L., Grabstanowicz, L. R.., Chen, C., Commet, S. M., Xu, T., Lu, J. & Liu, D. J. Highly efficient non-precious metal electrocatalysts prepared from one-pot synthesized zeolitic imidazolate frameworks. *Adv. Mater.* **26**, 1093–1097 (2014).
41 Wang, C., Waje, M., Wang, X., Tang, J. M., Haddon, R. C. & Yan, Y. Proton exchange membrane fuel cells with carbon nanotube based electrodes. *Nano Lett.* **4**, 345–348 (2004).
42 Jha, N., Ramesh, P., Bekyarova, E., Tian, X., Wang, F., Itkis, M. E. & Haddon, R. C. Functionalized single-walled carbon nanotube-based fuel cell benchmarked against US DOE 2017 technical targets. *Sci. Rep.* **3**, 2257 (2013).
43 Li, J. C., Hou, P. X., Zhao, S. Y., Liu, C., Tang, D. M., Cheng, M., Zhang, F. & Cheng, H. M. A 3D bi-functional porous N-doped carbon microtube sponge electrocatalyst for oxygen reduction and oxygen evolution reactions. *Energy. Environ. Sci.* **9**, 3079–3084 (2016).

Supplementary Information accompanies the paper on the NPG Asia Materials website (http://www.nature.com/am)